INL/CON-13-29588
PREPRINT

Overview of the BISON Multidimensional Fuel Performance Code

Technical Meeting on Modeling of Water-Cooled Fuel Including Design Basis and Severe Accidents

R. L. Williamson
J. D. Hales
S. R. Novascone
G. Pastore
D. M. Perez
B. W. Spencer
R. C. Martineau

October 2013

The INL is a
U.S. Department of Energy
National Laboratory
operated by
Battelle Energy Alliance

IAEA Technical Meeting: Modeling of Water-Cooled Fuel Including Design-Basis and Severe Accidents, October 28 to November 1, 2013, Chengdu, China

Overview of the BISON Multidimensional Fuel Performance Code

R. L. Williamson[a], J. D. Hales[a], S. R. Novascone[a], G. Pastore[a], D. M. Perez[a]
B. W. Spencer[a] , R. C. Martineau[a]

Abstract. BISON is a modern multidimensional multiphysics finite-element based nuclear fuel performance code that has been under development at the Idaho National Laboratory (USA) since 2009. A brief background is provided on the code's computational framework (MOOSE), governing equations, and material and behavioral models. Ongoing code verification and validation work is outlined, and comparative results are provided for select validation cases. Recent applications are discussed, including specific description of two applications where 3D treatment is important. A summary of future code development and validation activities is given. Numerous references to published work are provided where interested readers can find more complete information.

1. Introduction

BISON is a modern finite-element based nuclear fuel performance code that has been under development at the Idaho National Laboratory (USA) since 2009 [1]. The code is applicable to both steady and transient fuel behavior and can be used to analyze 1D (spherically symmetric), 2D (axisymmetric and plane strain) or 3D geometries. BISON has been used to investigate a variety of fuel forms including LWR oxide fuel [1], TRISO coated-particle fuel [2], and metallic fuel in both rod [3] and plate geometries.

This overview paper provides a brief background on the code's computational framework, governing equations, and material and behavioral models. Ongoing code verification and validation efforts are outlined. Recent applications are discussed with specific description of two applications where a 3D treatment is important. A summary of planned code development and validation activities is given. Numerous references to published work are provided where interested readers can find more complete information.

2. Background

BISON is built using the INL Multiphysics Object-Oriented Simulation Environment, or MOOSE [4]. MOOSE is a massively parallel, finite element-based framework to solve systems of coupled non-linear partial differential equations using the Jacobian-Free Newton Krylov (JFNK) method [5]. This enables investigation of computationally large problems, for example a full stack of discrete pellets in a LWR fuel rod, or every rod in a full reactor core. MOOSE supports the use of complex two and three-dimensional meshes and uses implicit time integration, important for the widely varied time scales in nuclear fuel simulation. An object-oriented architecture is employed which greatly minimizes the programming effort required to add new material and behavioral models.

[a] Fuel Modeling and Simulation Department, Idaho National Laboratory, Idaho Falls, Idaho, USA

The BISON governing relations currently consist of fully-coupled partial differential equations for energy, species, and momentum conservation. Users can select a subset of these equations (e.g., energy and momentum for thermomechanics analysis) within the input file. The code employs both nonlinear kinematics, which accounts for large deformation, and nonlinear material behavior. A detailed description of the nonlinear kinematics is provided in [1]. For nonlinear plasticity and creep, strains are calculated implicitly utilizing the radial return method; the specific procedure is outlined in [6].

Focusing principally on UO_2 fuel, models are included in BISON to describe temperature and burnup dependent thermal properties, solid and gaseous fission product swelling, densification, thermal and irradiation creep, fracture via relocation or smeared cracking, and fission gas production, generation, and release [1]. For TRISO coated-particle fuel, an empirical model is included to compute CO production, which can be added to released fission gas to affect particle pressure [2].

Recently an improved fission gas release model was implemented in BISON, based on the work of Pastore et al. [7]. While retaining a physics-based description of the relevant mechanisms, the model is characterized by a level of complexity suitable for application to engineering-scale nuclear fuel analysis and consistent with the uncertainties pertaining to some parameters. The treatment includes the fundamental features of fission gas behavior, among which are gas diffusion and precipitation in fuel grains, growth and coalescence of gas bubbles at grain faces, grain growth and grain boundary sweeping effects, thermal, athermal, and transient gas release. This model, as implemented in BISON, was recently compared to a variety of experiments from the FUMEX-II [8] and FUMEX-III [9] International Atomic Energy Agency (IAEA) Coordinated Research Projects (CRP) [10]. Comparison of results with available experimental data up to moderate burn-up, demonstrated an encouraging predictive accuracy, without any fitting applied to the model parameters.

Focusing initially on Zircaloy as a clad material, models are available for instantaneous plasticity, thermal and irradiation creep, and irradiation growth. The plasticity and creep models can be applied simultaneously, in cases where both phenomena are active.

Gap heat transfer is modeled in the traditional manner with the total conductance across the gap computed as a sum of the gas conductance, the increased conductance due to solid-solid contact, and the conductance due to radiant heat transfer [1]. This model is typically applied between the fuel and clad, but can also be used to simulate heat transfer between individual pellets, between a pellet and end cap, or between fracture surfaces.

Mechanical contact between materials is implemented through the use of node/face constraints, which prevent nodes on one side of an interface from penetrating faces on the other side of the interface. This is accomplished in a manner similar to that detailed by Heinstein and Laursen [11] and discussed in greater detail in [12]. Finite element contact is notoriously difficult to make efficient and robust in three dimensions and continuous effort is underway to improve the mechanical contact algorithms in BISON.

For LWR fuel, the pressure in the gap and plenum is computed assuming a single cavity volume and using the ideal gas law. The moles of gas, the temperature, and the cavity volume are free to change with time. The moles of gas at any time is computed as the original amount of gas

(computed based on original pressure, temperature, and volume) plus the amount in the cavity due to fission gas released. The gas temperature is computed as a weighted average of the pellet exterior and cladding interior surfaces, with weighting based on an approximation of the volume of gas contained between the solid surfaces. The cavity volume is computed as needed based on the evolving pellet and clad geometry.

A variety of other material models have been implemented in BISON, often by users needing a specific model not available in the material library. These include thermal models for MOX and U_3Si_2 fuel, thermal and mechanical models for HT9 stainless steel cladding, irradiation-induced strain and creep models for pyrolitic carbon, and an irradiation creep model for SiC. These models are described in more detail in the BISON theory manual [13]. As mentioned above, the object-oriented architecture employed in MOOSE/BISON significantly minimizes the programming required to add new material and behavior models.

3. Verification and Validation

From the beginning, the development of BISON has been accompanied by the creation of numerous verification tests in which specific features of the code are tested to see if they compute the correct analytical or known solution. There are currently over 800 regression tests in the MOOSE/BISON framework. During code development, these regression tests are run frequently on a variety of computer platforms, and the results are checked against trusted solutions.

An effort is also underway to assess BISON's capability to predict real fuel behavior, principally by comparison to data from a variety of instrumented LWR fuel rods. This assessment effort has been invaluable, leading to the discovery of development oversights and errors not apparent from the simpler regression tests. Additionally it has led to improved confidence in BISON's ability to predict nuclear fuel behavior.

To date, 21 assessment cases have been simulated with BISON, as summarized in Table 1. Indicated in the table are the measured quantities for comparison, namely fuel centerline temperature (FCT) at beginning of life (BOL), throughout life (TL) and during power ramps (Ramps), fission gas release (FGR), cladding elongation (Clad-Elong), and cladding outer diameter following pellet clad mechanical interaction (PCMI). Many of these assessment cases grew out of participation in the IAEA sponsored FUMEX-III Coordinated Research Project [9] and are priority cases from either FUMEX-II [8] or FUMEX-III. Other cases were chosen based on recommendations from nuclear fuel experts. This section summarizes comparisons for a selected set of the cases in Table 1, as identified with an asterisk, to give an overview of the BISON validation effort. A more detailed description of this activity is given in [14] and a comprehensive assessment paper is in preparation.

3.1 Beginning of Life Fuel Centerline Temperature

The IFA-431 and IFA-432 fuel assemblies were irradiated in the Halden Boiling Water Reactor from 1975 to 1977 and 1975 to 1984, respectively. Each assembly contained six instrumented rods, with centerline temperature instrumentation in the top and bottom ends of the fuel pellet stack. The test rods initially contained fresh UO_2 fuel. Three of the six rods (1, 2, and 3) from each experiment were used for Beginning of Life (BOL) temperature comparisons. All six rods

were meshed using 2D-RZ axisymmetric quadratic (quad-8) elements. For simplicity, the pellet stack was modeled as a smeared column containing thermocouple holes at the top and bottom, to best represent the actual fuel geometry.

TABLE 1. SUMMARY OF BISON LWR ASSESSMENT CASES

Experiment	Rod	FCT BOL	FCT TL	FCT Ramps	FGR	Clad-Elong	Clad-Dia (PCMI)
IFA-431*	1	X					
IFA-431*	2	X					
IFA-431*	3	X					
IFA-432*	1	X					
IFA-432*	2	X					
IFA-432*	3	X					
IFA-513	1	X	X				
IFA-513	6	X	X				
IFA-515.10	A1	X	X				
IFA-597.3	7			X		X	
IFA-597.3	8			X			
Risø-3*	AN3			X	X		
Risø-3	AN4			X	X		
FUMEX-II	27(1)				X		
FUMEX-II	27(2a)				X		
FUMEX-II	27(2b)				X		
FUMEX-II	27(2c)				X		
Risø-3*	GE7						X
OSIRIS	J12						X
REGATE							X
IFA-431 (3D)	4	X					

Fuel cracking occurs during the first rise to power, increasing the effective fuel volume and decreasing the gap width. The gap width and thus cracking have a strong influence on fuel temperature. Cracking is modeled in BISON using either a simple empirical relocation model or a more mechanistic smeared cracking model. For the BOL comparisons shown here, the empirical relocation model was used. Calibration of this model to a variety of experiments was considered in conjunction with this study, as described in Swiler et al. [15]. A relocation activation energy of 5 kW/m was used here based on this study.

Temperature comparisons during the first rise to power are significant since they isolate several important aspects of fuel rod behavior before complexities associated with higher burnups are encountered. For example, proper prediction of BOL centerline temperatures requires accurate models for the fuel and clad thermal conductivity, gap heat transfer, thermal expansion of both the fuel and the clad materials (to predict an accurate gap width), and fuel relocation.

Figure 1 compares measured and predicted BOL fuel centerline temperature for all six rods. Note that for IFA-432 Rod 2, only lower thermocouple comparisons are possible since the

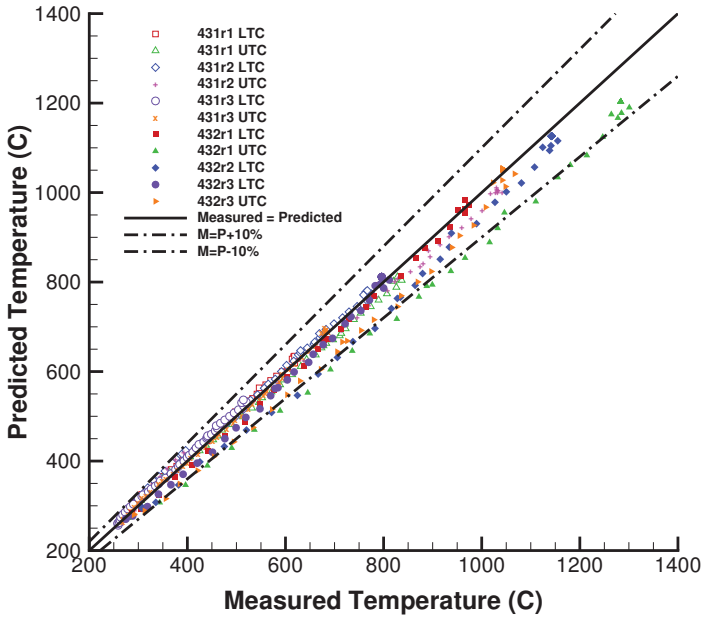

FIG. 1. Measured vs. predicted fuel centerline temperature for rods 1, 2, and 3 in IFA-431 and IFA-432. LTC and UTC stand for lower and upper thermocouples respectively.

gamma thermometer in the upper rod location failed to operate. The overall agreement is excellent, with only one rod falling outside of the +/-10% error band.

3.2 Fuel Temperature and Fission Gas Release During Ramp Testing

The Risø AN3 experiment was one of the FUMEX-II priority cases [8] and was conducted at the Risø DR3 water-cooled HP1 rig. This experiment utilized a re-fabricated fuel rod from a PWR fuel pin irradiated over four cycles. The re-fabricated rod was shortened and fitted with a fuel centerline thermocouple and pressure transducer. The re-fabricated (shortened) rod geometry was assumed for both the base irradiation and ramp test. The pellet stack was modeled as two smeared fuel blocks, with an annular block at the top to account for the thermocouple hole. The fuel and clad were modeled using a 2D-RZ axisymmetric quad-8 mesh.

Figure 2 compares the fuel centerline temperature and fission gas release to both experimental data and predictions from the well-known and validated codes TRANSURANUS and ENIGMA. Data for code comparisons were digitized from plots provided in the FUMEX-II final report [16]. In view of the uncertainties involved in FGR modeling, the predictions are very reasonable, both in terms of FGR value at the end of life and kinetics of the phenomenon. Fuel centerline temperature comparisons are excellent. The more accurate prediction of fission gas release observed with BISON leads to better fuel centerline temperature comparisons as gas release and fuel temperature are strongly coupled. Obviously this single rod comparison does not permit any general comparisons between BISON and other fuel performance codes.

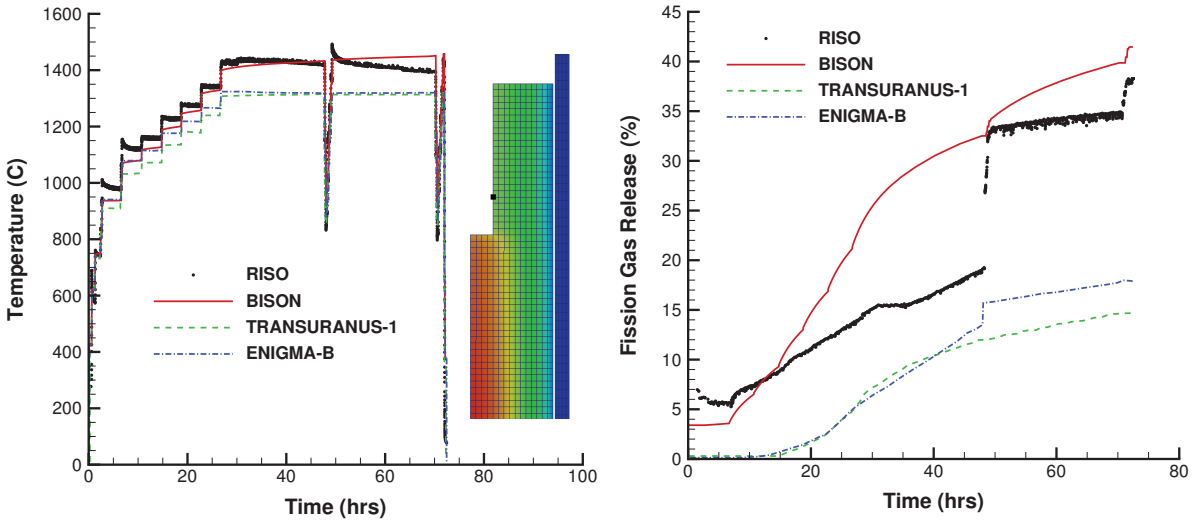

FIG. 2. Fuel centerline temperature and fission gas release comparisons during the Risø AN3 power ramp. Comparisons are included to experimental data and other code predictions. The contour plot shows a typical drilled fuel mesh (magnified 5X in the radial direction) with the dot indicating the comparison location.

3.3 Pellet Clad Mechanical Interaction

The Risø GE7 test was one of the FUMEX-III priority cases [9] also conducted at the HP1 rig under BWR conditions. This experiment utilized a fuel pin segment that was base irradiated over four reactor cycles and then bump tested. The segment was neither punctured nor opened for re-fabrication for the bump test. Although the axial power distribution during base irradiation was relatively flat, there was a significant axial power profile, weighted heavily to the bottom of the fuel segment, during the bump test. The rod segment contained 72 fuel pellets and was modeled assuming 2D-RZ axisymmetry with each pellet considered separately (discrete pellet mesh). Quadratic quadrilateral finite elements were used.

Comparison of the predicted and measured clad final outer diameter, as a function of rod length, is shown in Figure 3. BISON over-predicts the clad creep-down during base irradiation, resulting in a rod diameter approximately 10 μm less than measured values. The prediction, however, is very reasonable. Permanent clad deformation during the bump test is observed over roughly the bottom two-thirds of the rod. BISON predicts the shape of this deformation nicely. The high frequency oscillation in the BISON curve is a result of ridges formed in the cladding at pellet-pellet interfaces due to the hourglass shape of the pellets. Note that the amplitude of the ridges compare very well with that observed experimentally. The commonly observed ``bamboo'' profile along the clad length is obvious in a contour plot included in the figure, which shows the radial displacement on a short section of the deformed clad. Each displacement peak (red zone) corresponds to one of the peaks in the BISON predicted rod

diameter curve. Also included in Figure 3 are results from ENIGMA as provided by personnel at the National Nuclear Lab. BISON compares well with ENIGMA, which also over predicts the fuel creep-down resulting in an under prediction of the final fuel diameter.

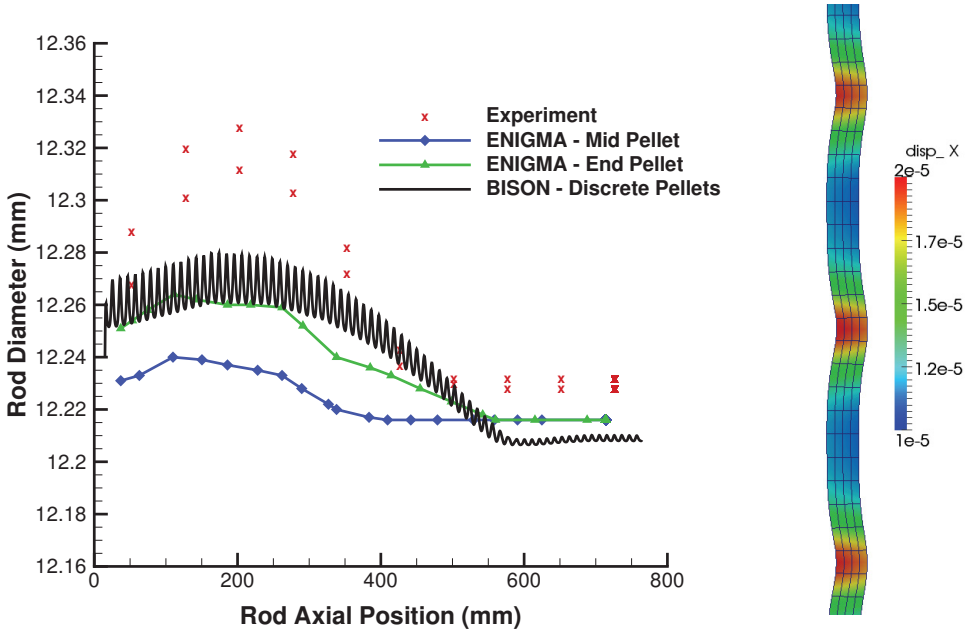

FIG. 3. BISON post-bump rod diameter predictions compared to measurements and ENIGMA calculations. Also shown are radial displacement contours for a short section of cladding. The radial mesh is scaled 2X and the displacements magnified 30x to improve visualization.

3.4 TRISO Coated-particle Fuel

Note that an additional BISON validation effort for TRISO coated-particle fuel, based on code comparisons to numerous benchmark cases from an IAEA CRP [17], was recently completed and is documented in [2].

4. Applications

BISON has been applied to a variety of LWR fuel rods using both smeared and discrete pellet meshing, and assuming both axisymmetric and 3D behavior (see [1, 14]). Additionally, the code has been applied to TRISO coated-particle fuel [2], fast oxide fuel, and metal fuel in both rod and plate form [3]. In this section, two LWR applications are described, in both cases where 3D analysis is important. The first considers fuel with a missing pellet surface and the second investigates the effect of fuel pellet eccentricity.

4.1 Simulation of Missing Pellet Surface Defects

4.1.1 Problem and Model Description

Local geometric irregularities in fuel pellets caused by manufacturing defects known as missing pellet surfaces (MPS) can in some circumstances lead to elevated cladding stresses that are sufficiently high to cause cladding failure [18, 19]. Accurate modeling of these defects can help understand and possibly prevent these types of failures.

To study the influence of MPS defects on the cladding, results from 1.5D or 2D fuel performance analyses are typically mapped to thermo-mechanical models that consist of a 2D plane-strain slice or a full 3D representation of the geometry of the pellet and clad in the region of the defect [20, 21]. There are three main potential sources of error due to mapping results from global fuel rod simulations to local 2D or 3D models of the defect. The first of these is that errors can be introduced in mapping results from a fuel rod model to provide the boundary conditions for a local model of the defect region. Secondly, the fuel/cladding system is influenced by multiple coupled physics, all of which influence both the global behavior of that system as well as the behavior in the region of a defect. These physics and behavior models are typically included in a fuel rod simulation, but may not necessarily be included in a local model of the region near the defect. Finally, the geometry of the MPS defect is inherently 3D. Problems can arise due to the use of reduced dimensionality models of the defect region.

To address the sources of error outlined above, BISON has been used to model short segments of fuel rods that include a pellet with a defect. A single 3D model is used to model both the global fuel performance and the local effects of the defect, so there is no need to map results between two models. The complete set of coupled physics and behavior models used in the fuel rod simulation is also used to model the region of the defect, and because the model is in 3D, its dimensionality is appropriate for the phenomena it is used to simulate. Note that this investigation is only summarized here and is described in greater detail in [22].

Figure 4 shows two finite element meshes of rod segments with imperfections used in this work. A constant-depth missing surface extends over the full depth of a pellet at the center of the five-pellet segment in each of these models. One case has a 0.25 mm deep defect, and the other has a 0.5 mm deep defect. Both of these models are run under the same conditions to study the effect of varying the imperfection depth. The models take advantage of a symmetry plane passing through the center of the defect, and boundary conditions are applied to enforce symmetry conditions. Both models have 106589 nodes and 22578 20-noded quadratic elements. Quadratic elements are used for both the fuel and the cladding because they smoothly represent 3D curved geometry for thermal and mechanical contact.

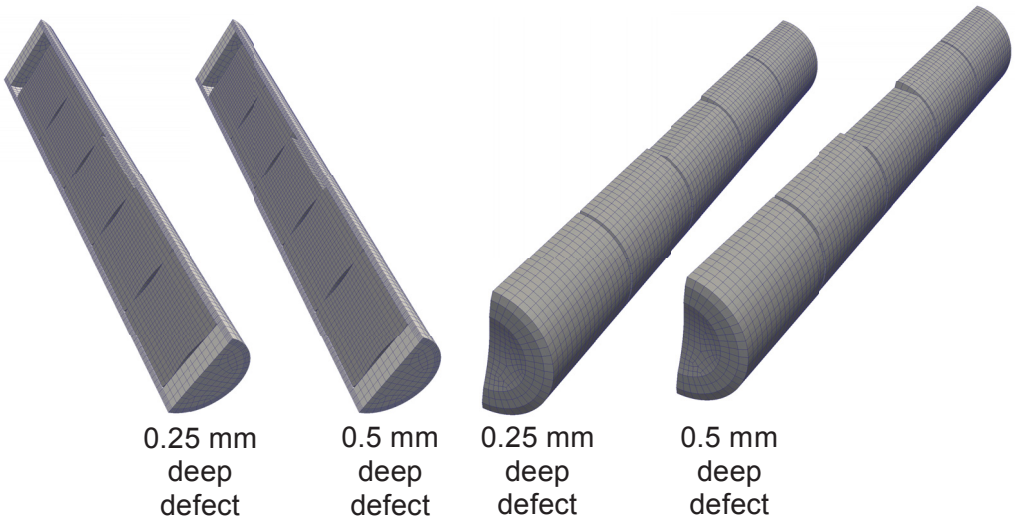

FIG. 4. Computational meshes of rod segments with a defective pellet.

Coupled heat conduction and solid mechanics equations are solved. The pellets have temperature and burnup-dependent conductivity and swelling, and are modeled as linear elastic with thermal expansion. The cladding material has constant thermal conductivity and a combined creep and plasticity model is used for the mechanical constitutive behavior. Cladding creep is dependent on both temperature and fast neutron flux. Fission provides a volumetric heat source to the fuel. Thermal conductance across the fuel/cladding gap is based on distance, roughness, gas composition, and surface emissivity. A flux boundary condition is used to model heat transfer from the cladding to the coolant. This boundary condition employs a constant convection coefficient to calculate the flux between the cladding surface, which has a calculated temperature, and the fluid, which has a prescribed temperature.

The fission rate is uniformly distributed both axially and radially. The idealized power history shown in Figure 5 is applied to both models and includes an initial power-up, base irradiation that includes holding the power constant for a time and then slowly ramping it down, and then a power ramp after 7e+7 seconds. The power ramp is expected to cause elevated stress and strain in the region of the defect due to pellet-clad mechanical interaction.

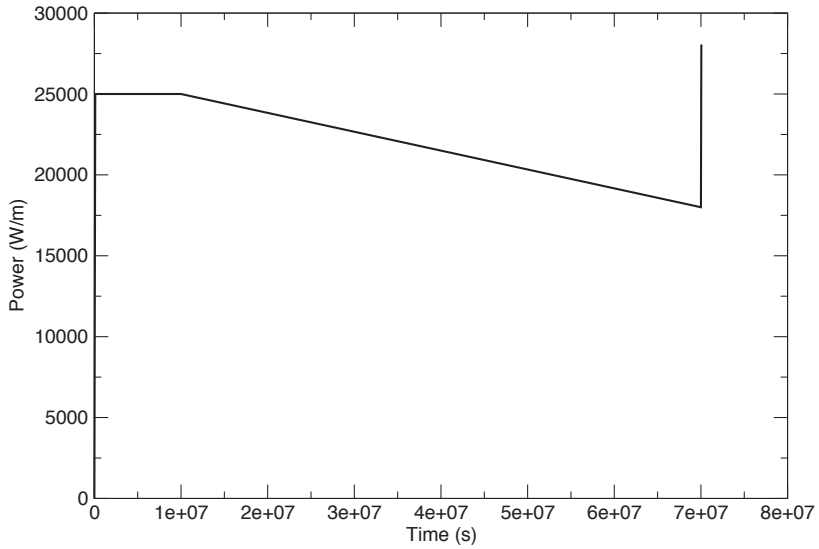

FIG.5. Idealized power history for the MPS analyses.

4.1.2 Results

The MPS defect causes elevated temperature at the center of the pellet and in the region of the pellet adjacent to the defect due to decreased conductance across the gap at the defect. The clad temperature is reduced in the area immediately across from the defect, and is elevated in neighboring areas. These effects can be seen in Figure 6(a), which shows the pellet and clad temperature at the end of the ramp, and in Figure 6(b), which shows just the clad, with displacements magnified 15x. As expected, the effects of the MPS defect are more pronounced with the deeper defect.

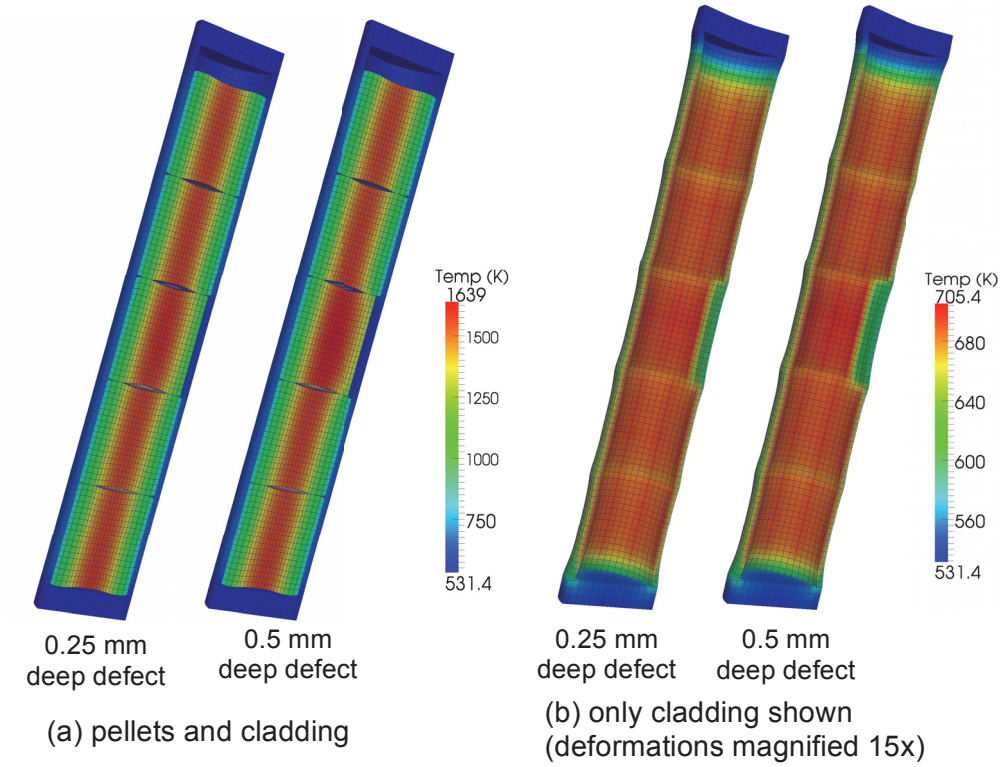

FIG. 6. Predicted temperature at end of power ramp.

The distance between the pellet and the clad is much greater adjacent to the MPS defect than it is for undamaged pellets. This causes a dramatic decrease in the conductance across the gap and a corresponding decrease in heat transfer between the pellet and clad adjacent to the defect. The temperature is thus elevated in the fuel near the surface with the defect. Because of the higher fuel temperature, the cladding temperature is elevated around the boundaries of the defect, where the gap conductance is unaffected by the defect. Immediately adjacent to the defect, the cladding temperature is significantly decreased because of the lower gap conductance.

The mechanical effects of the MPS defect are evident in contour plots of the von Mises stress and effective creep strain in the cladding, shown in Figures 7 and 8 respectively. These are shown with displacements magnified 15x at the end of the power ramp for the two different defect depths. For both cases, there are pronounced pellet-clad mechanical interaction (PCMI) effects. The clad across from the defect bends inward due to the coolant pressure, and is supported around the boundaries of the defect in the pellet containing the defect and on the rims of the pellets above and below the defect. These regions have high contact pressures and elevated stresses in the cladding. This region exhibits classical plate bending behavior, with high tensile stresses in the interior of the cladding and high compressive stresses on the exterior of the cladding at the center of the defect. Around the boundaries of the defect, the stresses are reversed, with high compressive stresses on the cladding interior and high tensile stresses on the cladding exterior.

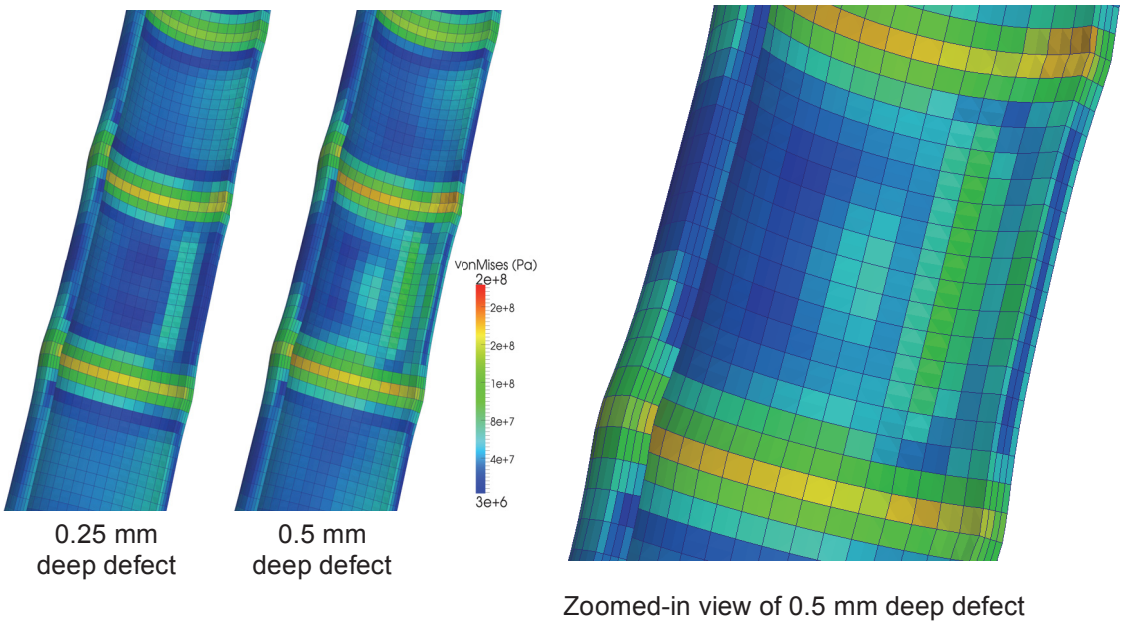

FIG. 7. Predicted von Mises stress at end of power ramp. Displacements are magnified 15x.

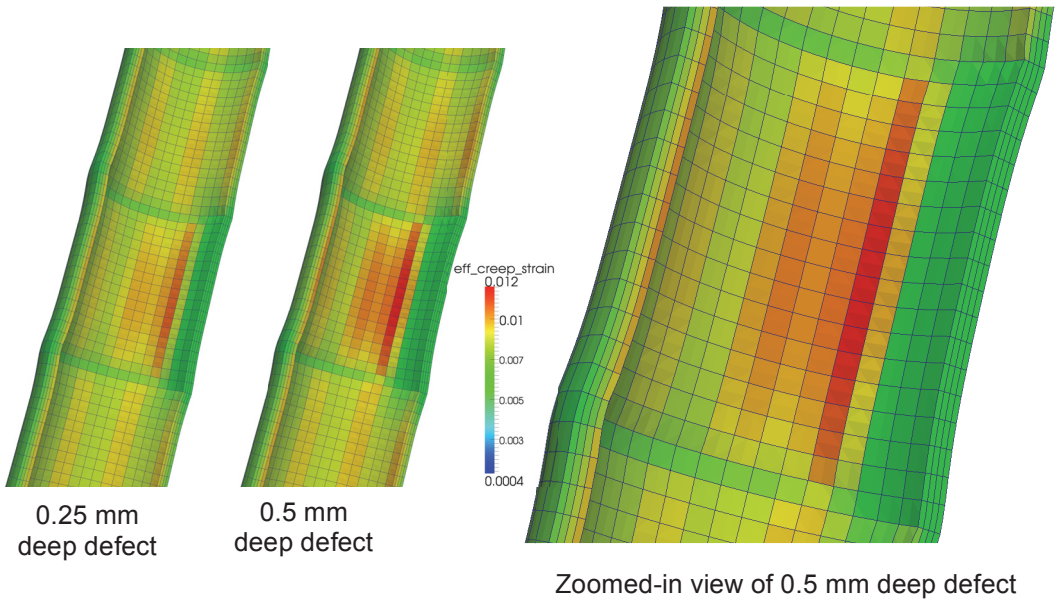

FIG. 8. Predicted effective creep strain at end of power ramp. Displacements are magnified 15x.

Cladding creep has a significant effect in relaxing stresses, both during the base irradiation and during the power ramp. As shown in Figure 8, the creep strains are low adjacent to the defect, but high around the boundary of the defect. This is largely due to the fact that temperatures are lower adjacent to the defect and higher around its edges.

Contact friction between the fuel and cladding is another effect that significantly influences cladding mechanical behavior near the defect. BISON currently models 3D frictionless and glued contact, but not frictional contact. Frictionless contact was used in the models presented here. The 0.5 mm deep defect model was also run with the baseline set of parameters, but with glued contact, which allows no tangential slip once mechanical contact is established. A comparison of the hoop stresses at the end of the power ramp for the frictionless and glued contact cases is shown in Figure 9. The increased constraint around the boundaries of the defect due to glued contact result in significantly higher tensile stresses on the cladding interior at the center of the defect. The actual result is likely bounded by the results obtained using the frictionless and glued contact models and clearly demonstrates the need for a frictional contact model. Work is currently underway to enable 3D frictional contact in BISON.

MPS defects clearly have a significant effect on the mechanical response in the cladding in the region of the defect. As shown in the analyses presented here, larger defects result in elevated stresses in the cladding. Stresses also increase with increased friction between the pellet and clad.

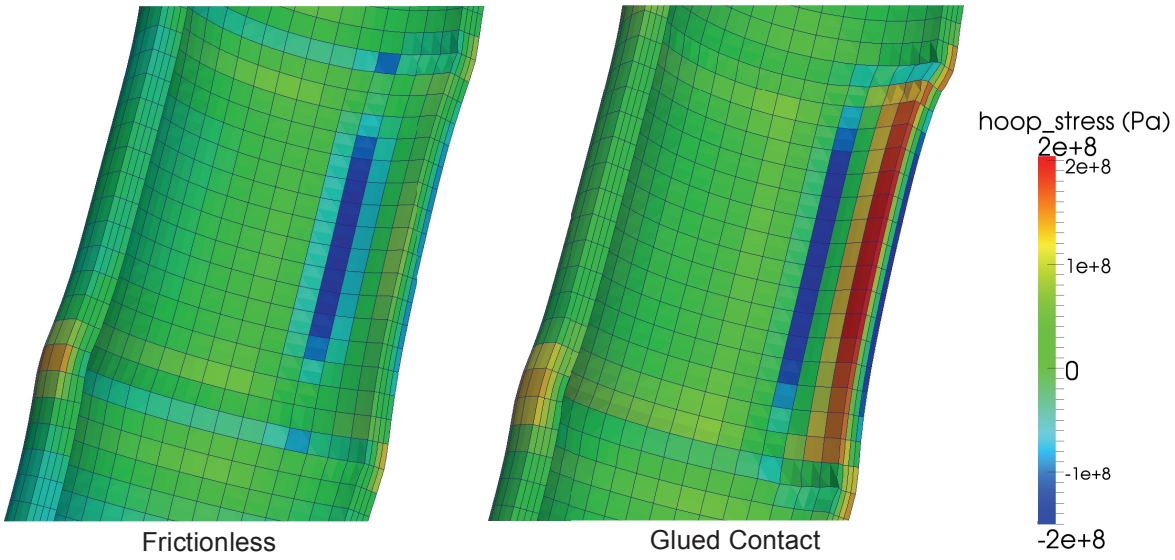

FIG. 9. Effect of frictionless versus glued contact on predicted hoop stress. Displacements are magnified 15x.

4.2 Simulation of Pellet Eccentricity Effects

4.2.1 Problem and Model Description

The Halden IFA-431 experimental assembly was briefly described in Section 3.1. Rod 4 of this series was designed to analyse the effects of xenon-filled gaps and pellet eccentricity. As shown schematically in Figure 10, the top and bottom of the fuel column were mechanically constrained with oversized pellets and molybdenum rods to ensure concentricity of the test pellets at the top of the fuel column and eccentricity of the test pellets at the bottom of the fuel column [23]. Due to the non-axisymmetric geometry of this experiment, it is not a viable candidate for analysis using most fuel performance codes, which are limited to, at most, 2D

analysis. This experiment was recommended by Halden researchers as one that could benefit from 3D analysis using BISON. The objective was to gain insight into the cause of differences between the measured temperature in concentric and eccentric rods. Note that this investigation is only summarized here and is described in greater detail in [24].

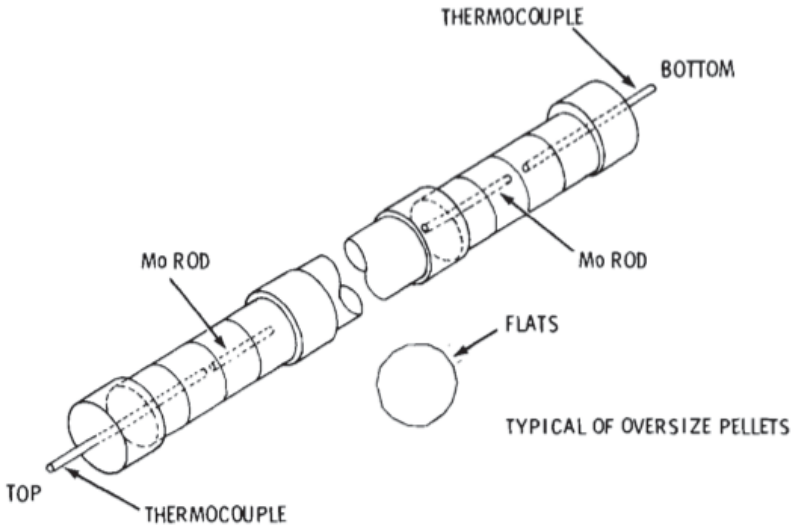

FIG. 10. IFA-431 Rod 4 fuel column schematic [23].

To simplify analysis, the top and bottom of the fuel column were modelled as two separate shortened rods. The 3D models of these rod sections used hex-20 elements, represented the fuel as a smeared column, and employed a symmetry plane passing through the fuel centreline. Figure 11 shows the concentric (left) and eccentric (right) meshes used for this comparison. A simplified power history was assumed, with the power ramped from 0 to 20 kW/m over a 90,000 second time period.

4.2.2 Results

Initial predictions indicated that BISON was over-predicting the fuel centreline temperature for both the concentric and eccentric comparisons. It was observed that the relocation model, with its default activation point of 19.7 kW/m, was not affecting the gap size except at the highest power levels in the study. Experimental observations such as [25], however, indicate that fuel cracking (and thus the onset of relocation) occurs at much lower power, on the order of 5 kW/m. This served as motivation for a study of the effects of the relocation activation power. The results of this parametric study, shown in Figure 12, concur that the relocation model should be activated at a power of roughly 5 kW/m, much lower than the default value. A recently reported more rigorous parametric study reached a similar conclusion [15].

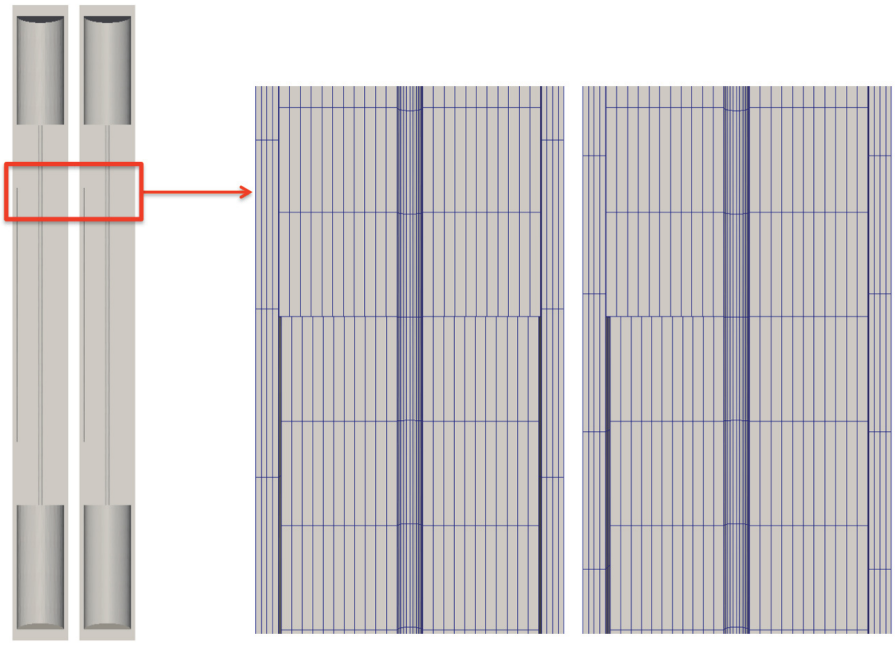

FIG. 11. IFA-431 Rod 4 3D half symmetry meshes for concentric (left) and eccentric (right) sections.

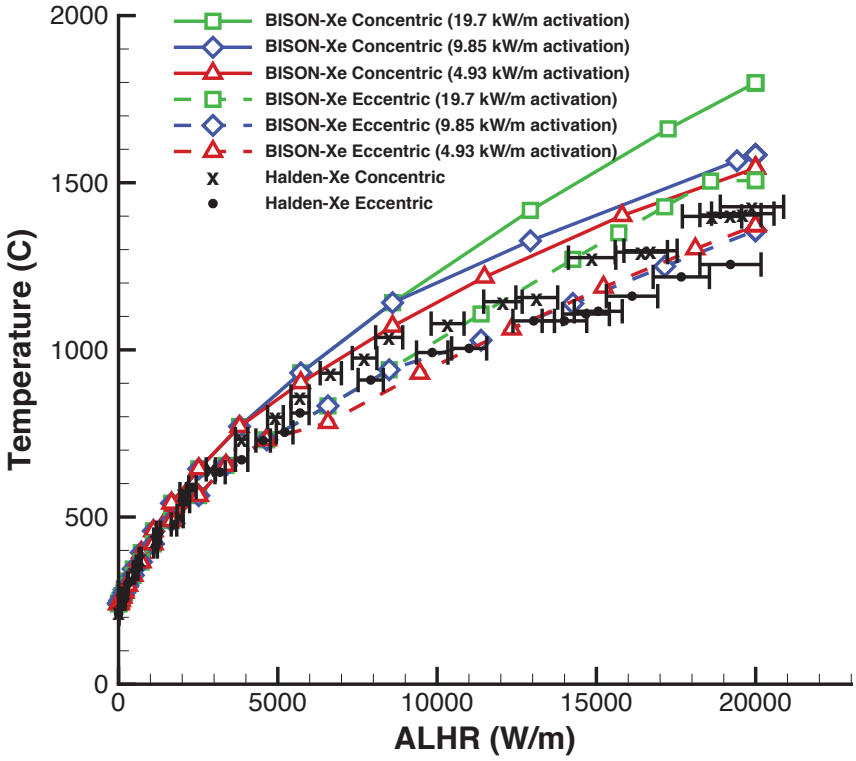

FIG. 12. Fuel centreline temperature comparisons for concentric (solid lines) and eccentric (dashed lines) pellets with varying relocation activation threshold power. Error bars are +/- 5% power uncertainty.

Both the experimental and analysis results indicate that the fuel centreline temperature measured is lower in the eccentric pellets than the concentric pellets. This raises the question of whether this is because fuel temperatures in the eccentric pellets are lower, or because the thermocouple is located away from the hottest location in the fuel. Figure 13 shows a side-by-side comparison of the concentric and eccentric pellets, accompanied by a plot of the fuel temperature along the cross-section of the pellets at the mid-plane of the fuel. It can be seen that the concentric test pellets are indeed hotter, and also that the thermocouple is not at the hottest location in the eccentric pellets, which is offset from the centreline due to pellet eccentricity. The peak fuel temperature of the concentric pellets occurs, as expected, at the fuel centre (TC location) and is ~2074 K. The peak temperature for the eccentric pellets occurs at 1.412 mm to the left of the TC location (refer to Figure 13) and is ~1884 K.

The comparison confirms with modern 3D analysis tools that the measured temperature difference between concentric and eccentric pellets is not an artefact and provides a quantitative explanation for the difference. The comparison further demonstrates that, although an old experiment, IFA-431 Rod 4 is clearly still of value since it provides a rare opportunity to validate 3D behavior in a fuel performance code.

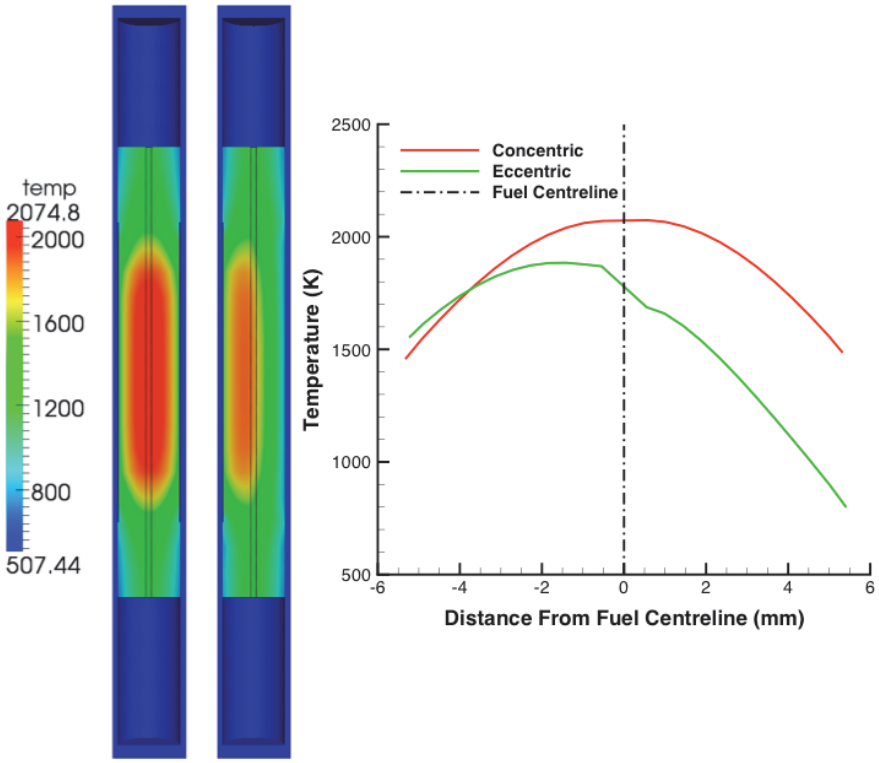

FIG. 13. Temperature contour plot of the concentric (left) and eccentric (right) pellets and fuel temperature along the cross-section of the pellets, at the fuel mid-plane.

5. Summary of Future Efforts

5.1 Verification, Validation and Uncertainty Quantification

Although significant verification and validation work has been completed, much work remains. Enlarging the validation base will be a major focus going forward, with continuing work on cases from the FUMEX-II and FUMEX-III CRPs. Collaborations have been developed with the Halden Reactor Project and the National Nuclear Laboratory to enlarge and hasten this effort. Because BISON is under active development, a system is being developed to frequently run all assessment cases and compare results to those from prior code versions. Sensitivity and uncertainty quantification analyses will continue.

5.2 Code Development

Active capability development also continues with BISON. For general fuel behavior analysis, priorities include a more robust and efficient thermomechanical contact model, improved fracture capabilities (both smeared and discrete) and development of a more extensive set of material models.

Efforts are also underway to enhance BISON to model accident behavior. Much of the necessary capability is inherent in the code, including transient operators with adaptive time stepping, arbitrary geometry with large deformation mechanics, and fully-coupled physics with implicit numerics. Development will continue on improved fission gas modeling, specifically coupling gas release to fuel swelling and implementing a burst release model. With regards to cladding behavior, models will be included for temperature and strain rate dependent plasticity, high temperature creep, hydrogen diffusion and embrittlement prediction, and rapid steam oxidation including a moving material interface.

ACKNOWLEDGEMENTS

The submitted manuscript has been authored by a contractor of the U.S. Govern-ment under Contract DE-AC07-05ID14517. Accordingly, the U.S. Government retains a non-exclusive, royalty-free license to publish or reproduce the published form of this contribution, or allow others to do so, for U.S. Government purposes.

REFERENCES

[1] WILLIAMSON R. L., HALES J. D., NOVASCONE S. R., TONKS M. R., GASTON D. R., PERMANN C. J., ANDERS D., MARTINEAU R. C., Multidimensional multiphysics simulation of nuclear fuel behavior, Journal of Nuclear Materials, **423** (2012) p. 149–163.

[2] HALES J. D., WILLIAMSON R. L., NOVASCONE S. R., PEREZ D. M., SPENCER B. W., PASTORE G., Multidimensional multiphysics simulation of TRISO particle fuel, Journal of Nuclear Materials, **443**, (2013) p. 531–543.

[3] MEDVEDEV P., Fuel performance modeling results for representative FCRD irradiation experiments: Projected deformation in the annular AFC-3A U-10Zr fuel pins and comparison to alternative designs. Technical Report INL/EXT-12-27183 Revision 1, Idaho National Laboratory, (2012).

[4] GASTON D., NEWMAN C., HANSEN G., LEBRUN-GRANDIE´ D., MOOSE: A parallel computational framework for coupled systems of nonlinear equations, Nuclear Engineering and Design, **239**, (2009) p. 1768–1778.

[5] KNOLL D. A., KEYES D. E., Jacobian-free Newton-Krylov methods: A survey of approaches and applications, Journal of Computational Physics, **193(2)**, (2004) p. 357– 397.

[6] HALES J. D., NOVASCONE S. R., WILLIAMSON R. L., GASTON D. R., TONKS M. R, Solving nonlinear solid mechanics problems with the Jacobian-free Newton Krylov method. CMES: Computational Modeling in Engineering &. Science, **84(2)** (2012) p. 123–154.

[7] PASTORE G., LUZZI L., DI MARCELLO V., VAN UFFELEN P. Physics-based modelling of fission gas swelling and release in UO_2 applied to integral fuel rod analysis, Nuclear Engineering and Design, **256** (2013) p. 75–86.

[8] KILLEEN J. C., TURNBULL J. A., SARTORI E., Fuel modelling at extended burnup: IAEA coordinated research project FUMEX-II, Proceedings of the 2007 International LWR Fuel Performance Meeting, San Francisco, California, Paper 1102, Sept. 30–Oct. 3 (2007).

[9] Improvement of Computer Codes Used for Fuel Behavior Simulation (FUMEX-III), IAEA-TECDOC-1697, International Atomic Energy Agency, (2013).

[10] PASTORE G., HALES J. D., NOVASCONE S. R., PEREZ D. M., SPENCER B. W., WILLIAMSON R. L., Analysis of fission gas release in LWR fuel using the BISON code, 2013 LWR Fuel Performance Meeting – TopFuel, Charlotte, NC, September 15–19 (2013).

[11] HEINSTEIN M., LAURSEN T., An algorithm for the matrix-free solution of quasistatic frictional contact problems, International Journal of Numerical Methods in Engineering, **44** (1999) p. 1205–1226.

[12] HALES J. D., ANDRS D., GASTON D. R., Algorithms for thermal and mechanical contact in nuclear fuel performance analysis, Proceedings of the International Conference on Mathematics and Computational Methods Applied to Nuclear Science and Engineering, Sun Valley, Idaho, May 5-9 (2013).

[13] HALES J. D., NOVASCONE S. R., PASTORE G., PEREZ D. M., SPENCER B. W., WILLIAMSON R. L., BISON theory manual: The equations behind nuclear fuel analysis, Technical Report, Idaho National Laboratory (2013).

[14] PEREZ D. M., WILLIAMSON R. L., NOVASCONE S. R., LARSON T. K., HALES J. D., SPENCER B. W., PASTORE G., An evaluation of the nuclear fuel performance code

BISON, Proceedings of the International Conference on Mathematics and Computational Methods Applied to Nuclear Science and Engineering, Sun Valley, Idaho, May 5-9 (2013).

[15] SWILER L. P., WILLIAMSON R. L., PEREZ D. M., Calibration of a fuel relocation model in BISON, Proceedings of the International Conference on Mathematics and Computational Methods Applied to Nuclear Science and Engineering, Sun Valley, Idaho, May 5-9 (2013).

[16] Fuel modeling at extended burnup (FUMEX-II), IAEA-TECDOC-1687, International Atomic Energy Agency (2012).

[17] Advances in high temperature gas cooled reactor fuel technology, IAEA-TECDOC-1674, International Atomic Energy Agency (2012).

[18] ALESHIN Y., BEARD C., MANGHAM G., MITCHELL D., MALEK E., YOUNG M., The effect of pellet and local power variations on PCI margin, Proceedings of Top Fuel 2010, Orlando, FL, USA, September (2010).

[19] GROESCHEL F., BART G., MONTGOMERY R., YAGNIK S. K., Failure Root Cause of a PCI Suspect Liner Fuel Rod, IAEA Technical Meeting on Fuel Failure in Water Reactors: Causes and Mitigation, Bratislava, Slovakia, June 17-21 (2002).

[20] LEE J.S., YOO J.S., KIM H.K., The Mechanical Behavior of Pellet-Cladding with the Missing Chip under PCMI Loadings during Power Ramp, Proceedings of the 2007 International LWR Fuel Performance Meeting, Paper 1022, San Francisco, CA, Sept. 30-Oct. 3 (2007).

[21] KHVOSTOV G., LYON W., ZIMMERMAN M. A., Application of the FALCON code to PCI induced cladding failure and the effects of missing pellet surface, Annals of Nuclear Energy, **62** (2013) p. 398-412.

[22] SPENCER B. W., HALES J. D., NOVASCONE S. R., WILLIAMSON R. L., 3D Simulation of Missing Pellet Surface Defects in Light Water Reactor Fuel Rods, Proceedings of Top Fuel 2012, Manchester, United Kingdom, September 2-6 (2012).

[23] WILLIFORD R. E., HANN C. R., Effects of Fill Gas Composition and Pellet Eccentricity, Technical Report BNWL-2285/NRC-1&3 (1977).

[24] HALES J. D., PEREZ D. M., WILLIAMSON R. L., NOVASCONE S. R., SPENCER B. W., MARTINEAU R. C., Validation of the BISON 3D fuel performance code: Temperature comparisons for concentrically and eccentrically located fuel pellets, Enlarged Halden Programme Group Meeting: Proceedings of the Fuels and Materials Sessions, Volume HPR-378, Storefjell Resort Hotel, Norway, March 10–15 (2013).

[25] OGUMA M., Cracking and relocation behaviour of nuclear fuel pellets during rise to power, Nuclear Engineering and Design, **76** (1983) p. 35-45.